Advances in Environmental Technology 1 (2016) 11-24

Advances in Environmental Technology

journal homepage: http://aet.irost.ir

Preparation and characterizations of CuO doped ZnO nano-structure for the photocatalytic degradation of 4-chlorophenol under visible light

Afsaneh Shokri, Mohsen Mehdipour Ghazi*

Faculty of Chemical, Petroleum, and Gas Engineering, Semnan University, Semnan, Iran

ARTICLE INFO

Article history:
Received 17 September 2015
Received in revised form
16 July 2016
Accepted 7 August 2016

Keywords:
CuO doped ZnO
Photocatalytic degradation
Visible light
4-Chlorophenol

ABSTRACT

In the present investigation, a ZnO nanostructure was synthesized by means of precipitation and sonochemical methods. The X-ray diffraction (XRD) pattern indicated that the wurtzite structure of ZnO had a hexagonal symmetry and there was no impurity. The average ZnO particles crystallite size was calculated at about 41 nm. The SEM and TEM images revealed nanostructure ZnO particles with a cauliflower-like and rod morphology with dimensions of 85, 79 and 117 nm. In order to investigate the increment of ZnO photoactivity under visible light, the CuO doped ZnO nanostructures were fabricated by a wet impregnation method using copper oxide as the copper source and ZnO as the precursor. The XRD analysis confirmed that the CuO phase was present in the as-prepared sample and the average size of nano crystalline decreased to about 36 nm. The DRS spectra indicated the extended absorption of CuO-ZnO to the visible range as a result of band gap reduction to 2.9 eV (in comparison of 3.2 eV in ZnO). In order to investigate the photocatalytic activity of the synthesized photocatalyst, the degradation of 4-Chlorophenol under visible light was performed. Sixteen experiments using full factorial were executed by adjusting four parameters (amount of catalyst, initial concentration of 4-Chlorophenol, pH, and time of irradiation). An empirical expression was proposed and successfully used to model the photocatalytic process with a high correlation, and an optimal experimental region was also obtained. According to the developed model for degradation and the subsequent ANOVA test using Design Expert software, the time of irradiation with a 46.57% effect played the most important role in the photocatalytic activity, while the influences of parameters on each other were negligible. Optimal experimental conditions for 4-Chlorophenol concentration (0.01 g/L) were found at an initial pH =8 and a catalyst loading of 0.07 g/L. The results indicated that CuO-ZnO can remove 95% of 4-chlorophenol from water under optimal conditions.

1. Introduction

In recent years, hazardous water soluble compounds have gained worldwide attention [1]. Conventional treatment technology such as biological treatment, chemical precipitation, activated carbon adsorption, ion-exchange process, and chlorination is not always suitable and has several drawbacks. They transfer the pollutants from one medium to another and thus, additional treatment is required. Also, they usually require a longer treatment time. Sometimes they even generate by-products that are more toxic than the primary contaminants [2-4]. Semiconductor photocatalysis is the most suitable alternative method which has been developed due to its efficiency in the total destruction of contaminants, environmentally friendly procedure, economic appeal, and non-selective [5, 6]. As shown in Figure 1, this process is done by using a semiconductor photocatalyst, an energetic radiation source, and an oxidizing agent; it is largely dependent on the in-situ photogeneration of hydroxyl radicals that affect the destruction of persistent pollutants

*Corresponding author. Tel.: +98-2331533922
E-mail address: mohsenmehdipour@semnan.ac.ir

by converting them into mineral products such as CO_2 and H_2O.

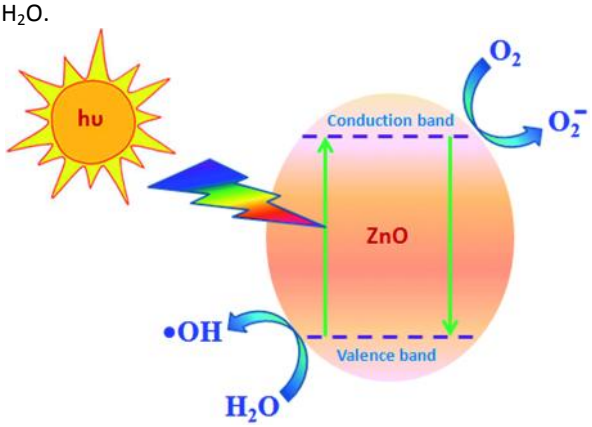

Fig. 1. Schematic diagram of semiconductor photocatalysis

Although TiO_2 has been the most studied photocatalyst, but it is expensive and not economically feasible for large-scale wastewater treatment [7]. ZnO is a better alternative and sometimes ranked higher than TiO_2 in photocatalytic efficiency [8,9]. Although the band gap energy (3.2 ev) and mechanism of photodegradation by ZnO are similar to TiO_2, the biggest advantage of ZnO is that it absorbs over a larger fraction of the solar spectrum. [10]. There are a variety of strategies to tailor the morphology of ZnO nanoparticles, control its growth direction, reduce its agglomeration, and enhance its photo catalytic properties [11]. Moreover, it is relatively low-cost, stable, and has large initial rates of activities as well as many active sites with high surface reactivity leading to high photocatalytic performance [12]. Some researchers have combined an oxide semiconductor with different energy levels to achieve more photocatalytic efficiency as a result of a vectorial transfer of photogenerated electrons and holes from a semiconductor to another and prevent recombination of photogenerated electrons and holes [13-16]. Furthermore, there are many reports regarding the use of CuO/ZnO during methanol synthesis, hydrogen production, and gas sensor [17-19] but few accounts concerning its use for photodegradation. ZnO is an n-type (electron-rich) large band gap (3.2 ev) semiconductor while CuO is a p-type (hole-rich) narrow band gap (1.7 eV) and their composite forms a p–n junction in the interface as a space-charge region. The electrons are diffused from a p-type (CuO) to an n-type (ZnO) semiconductor and the holes from an n-type to a p-type semiconductor. The p–n junction occurs as an inner electric field by the equilibrium of electron and hole diffusion, which improves the photocatalytic activity [20]. Therefore, nanostructures (CuO/ZnO) may pave the way for various new applications. Cu-doped ZnO nanomaterials permit the tuning of chemical and physical properties by the incorporation of the dopant in the lattices of ZnO. The possibility of band gap engineering is reported by Chang et al. in the doped ZnO by the barrier layers which will facilitate radiative recombination by carrier confinement. Cu doped ZnO nano powders with 40 nm size have been synthesized by the solution combustion method which showed a red shift and narrowing of band gap. Even though much research has been carried out on the Cu doped ZnO system, most of the works concern the thin films, and comprehensive studies of the structural and optical properties of Cu doped ZnO nano powders are still scanty. The effect of Cu on its structural, optical, and morphological properties has been studied extensively. Further, the size dependent properties of the nanoparticles are correlated with the band gap [21-26]. ZnO can be useful for the photocatalytic oxidation of different organic contaminants and the complete mineralization of environmental pollutants [10,14,15,20, 27-31]. Between the organic contaminants, chlorophenols (despite their low concentration due to their variety, high toxicity, bio-recalcitrant structure, and persistence) have elevated toxicological risk [32]. The US Environmental Protection Agency (US EPA, 1987) and the European Union directive (EEC, 1990) have introduced chlorophenols as “priority pollutants”, which means that constant monitoring of the aquatic environment is necessary; also, the maximum permissible value of these compounds in the water supply is 0.5 mg/L [33]. The solubility of phenol derivatives is shown in Table 1.

Table 1. Solubility of phenol and its chloro and nitro-derivatives in water [18].

Compound	Solubility (g/100g)
Phenol	9.48
o-chlorophenol	2.04
m-chlorophenol	2.25
p-chlorophenol	2.77
o-nitrophenol	0.21
m-nitrophenol	2.19
p-nitrophenol	1.34

In particular, 4-Chlorophenol (4-CP) has the highest solubility and is generated as a by-product of paper and pulp, pharmaceutical, dyestuff, agrochemical industries, and waste incineration; it is a hazardous water soluble compound due to its toxicity and non-biodegradability. In these industries, the concentration of 4-CP in wastewaters is in the level of 300-500 mg/L [9, 34]. In the present study, the ZnO nanostructures were first synthesized via a simple sonochemical method; then, in order to enhance photocatalytic efficiency under visible light, the prepared ZnO nanostructures were doped with CuO by the wet impregnation method. These prepared nano powders were used for the photodegradation of 4-CP. The effect of operating variables such as catalyst doses, initial

concentration of pollutant, pH, and time of irradiation were investigated.

2. Materials and method

2.1. Materials

All chemicals used in this study were of analytical grade and Millipore water was used throughout all experiments. Zinc acetate [$Zn(CH_3COO)_2.2H_2O$], Ammonia [$NH_3.H_2O$ 25%], sodium hydroxide [NaOH] and Copper sulfate [$CuSO_4.5H_2O$] were purchased from Merck, Germany. Furthermore, 4-CP as a model pollutant was purchased from the Sigma-Aldrich Company, and its chemical structure and characteristics are given in Table 2.

Table 2. Characteristics and chemical structure of 4-CP

Other name	4-Hydroxychlorobenzene Parachlorophenol p-chlorophenol
Formula	C_6H_5ClO
Molecular Weight	128.56 g/mol
Melting point	41 – 44 °C
Initial boiling point	220 °C
maximum absorption(λ_{max})	279 nm
Structure	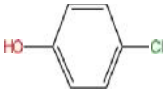

2.2. Preparation of nano ZnO

All the processes were carried out at room temperature without any specific conditions. First, zinc acetate was dissolved in ammonia (11 g in 100 mL). Then 4g sodium hydroxide was added to the solution. After that, deionized water was added until the final concentration became a 1M Zn^{2+} solution. The prepared solution was placed under ultrasonication for 60 min. The resulting white color product was centrifuged (5 min, 4000 rpm) and then washed three times with distilled water. The obtained white precipitate was dried in an oven at 60 °C for 24 h [35].

2.3. Preparation of the CuO/ZnO photocatalyst

After synthesizing and characterizing the ZnO particles, the doped zinc oxide powders were synthesized by the wet impregnation method [15]. First, about 1g of the ZnO nano particles was calcined at 400 ^{o}C for 5h. Then the mixture of nano ZnO and $CuSO_4.5H_2O$ (0.441g) was stirred for 48h and dried in an oven at 80 ^{o}C for 24h. The dried solids were calcined at 400 ^{o}C for 5h.

2.4. Characterization techniques

The crystallographic information of undoped and doped ZnO nanostructure was characterized by X-ray diffraction (XRD) (Bruker AXS, D8-Advance, Cu kα radiation, λ = 0.15418 nm). The surface morphology and the size of ZnO were analyzed by SEM and transmission electron microscopy (TEM). The diffuse reflectance spectra of the CuO/ZnO was recorded within the wavelength range 200–800 nm using a UV–vis spectrophotometer (UV-Vis. Shimadzu 1650-PC Spectrophotometer). Also, the light intensity of lamps was measured with lux meter (HT-309).

2.5. Photocatalytic experiments

The photocatalytic experiments were conducted under ambient atmospheric conditions in a batch reactor placed over a magnetic stirrer. A 500 W tungsten halogen lamp served as the light source (distance between experimental solution and light source is 15 cm). To increase the efficiency of the photocatalytic processes and complete degradation of 4-CP, the reactor was aerated during the experiments. In order to ensure adsorption/desorption equilibrium, the solution was stirred for about 45 min in darkness, prior to the irradiation. Figure 2, shows the schematic of the experimental system.

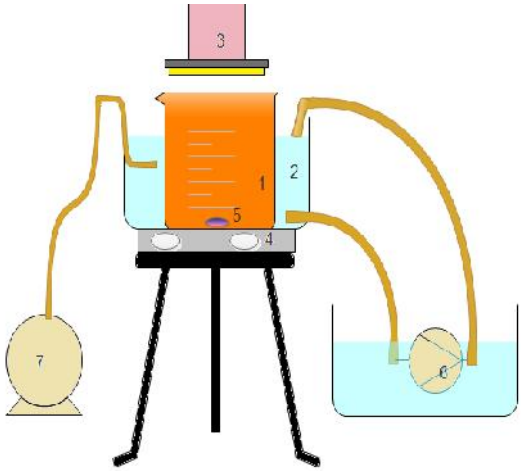

Fig. 2. The schematic of experimental system: 1. Batch reactor, 2. Cooling water, 3. Lamp, 4. Stirrer, 5. Magnet, 6, pomp, 7. Air pump.

2.6. Multivariate experimental design

Design of experiments (DOE) is a systematic, rigorous approach to problem-solving that applies principles and techniques at the data collection stage to ensure the generation of valid, defensible, and supportable scientific conclusions. In addition, all of this is carried out under the constraint of a minimal expenditure of experimental runs, time, and money. In this study, Design-Expert software (Version7) was used for computational analysis to obtain a mathematical model for the photodegradation of 4-CP. Taking into consideration the percent of the degradation

pollutant as a response, four main factors influencing the responses and their range were chosen: initial pollutant concentration (0.01–0.05 g/L), catalyst concentration (0.01–0.07 g/L), pH of reaction mixture (6–8), and irradiation time (60-240 min). Using these four factors, two levels of full factorial design of experiment technique for 16 sets of experiments were designed.

3. Results and Discussion

3.1. Characterization of ZnO nanostructures

The XRD pattern of synthesized ZnO is shown in Figure 3. The peaks observed in this model were in good agreement with the reference pattern corresponding to hexagonal wurtzite structure zinc oxide [JCPDS 36-1451, a = 0.326 nm, c = 0.522 nm]. The absence of other peaks indicated the absence of any impurities.

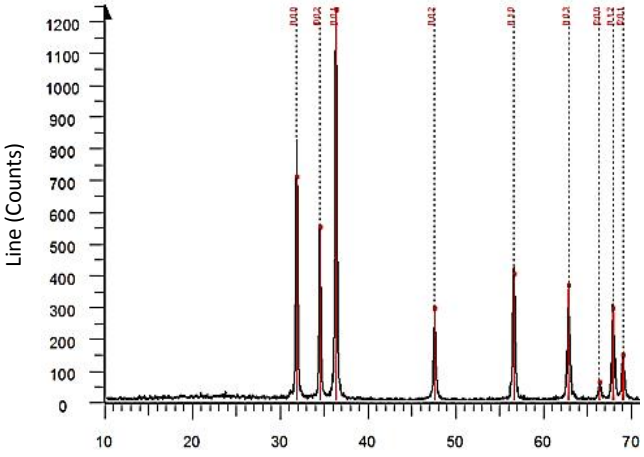

Fig. 3. XRD pattern of synthesized ZnO

The crystallite sizes of the ZnO nanostructure could be estimated by the Debye-Scherrer equation as follows [35]:

$$D = \frac{k\lambda}{\beta Cos\theta} \quad (1)$$

Where D is the average crystallite size (nm), λ is the wavelength of the X-ray radiation, β is the peak width at half maximum intensity in radians, k is a constant equal 0.93 [33], and θ is the half diffraction angle. The (101) plane (the strongest) was selected to calculate the crystallite size of ZnO nanostructures, and the estimated value was 41nm after 60 min ultrasonicaton. Figure 4, shows the morphological evolution from ZnO nanostructures. The morphology observed for the prepared ZnO nanostructure included cauliflower-like and rod shapes.

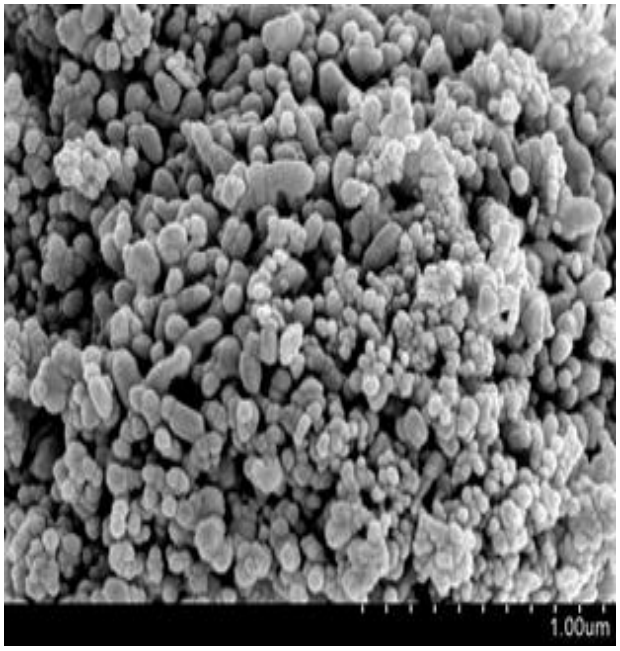

Fig. 4. SEM image of synthesized ZnO

Figure 5 shows the TEM images of the ZnO nanoparticles. It was evident that the dimensions of the synthesized ZnO were about 85, 79 and 117 nm. Figure 6 shows the XRD pattern of CuO/ZnO that indicated a CuO cluster present in the crystals of the ZnO nanoparticles. The estimated crystallite sizes of CuO/ZnO from Equation 1 were about 36nm. Thus, doping reduced the crystal size rather than the pure ZnO.

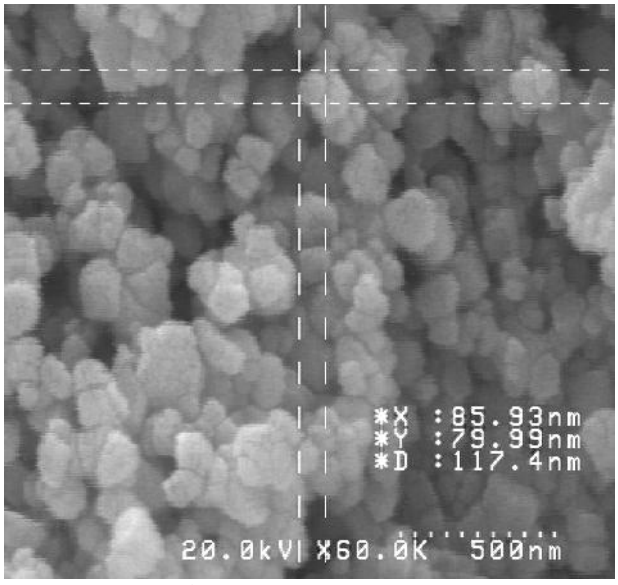

Fig. 5. TEM image of synthesized ZnO

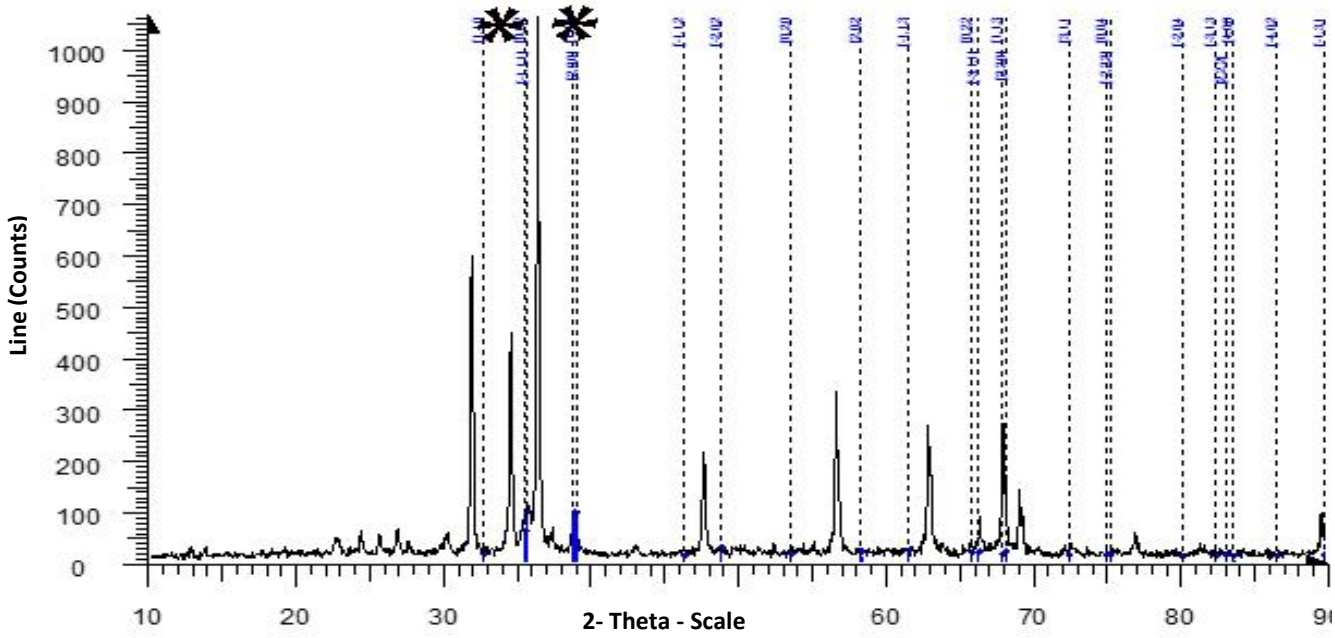

Fig. 6. XRD patterns of CuO/ZnO (Peaks of doped CuO was shown as *)

3.2. Characterization of CuO/ZnO nanophotocatalyst

The diffuse reflectance (R%) spectra of the CuO/ZnO nano-photocatalyst after the Kubelka-Munk (Equation 2) treatment are shown by Tauc's plots (Equations 2,3) in Figure 7. The intersection between the linear fit and the photon energy axis gives the value of band gap energy (E_g) [36,37].

$$K = \frac{(1-R)^2}{2R} \quad (2)$$

$$Khv = (hv - E_g)^2 \quad (3)$$

The E_g of CuO/ZnO of 2.9 eV was less than pure ZnO (E_g=3.2 eV). Thus, ZnO coupled with CuO can be activated at higher wavelengths in the visible range.

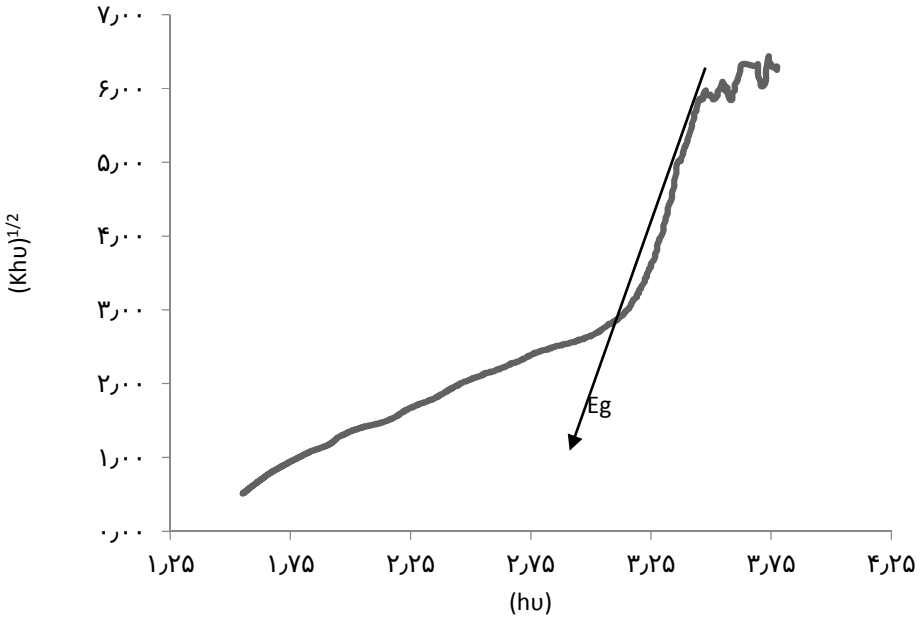

Fig. 7. Tauc's plot of CuO/ZnO nanophotocatalyst

The FTIR analysis of CuO/ZnO is given in Figure 8. This technique was used to obtain information about the material chemical bonding. It was used to identify the elemental constituents of a material. The broad absorption peaks around 3460 cm^{-1} and 1130 cm^{-1} were attributed to the normal polymeric O–H stretching vibration of H_2O in the Cu–Zn–O lattice [38]. Another sharp peak around 1604 cm^{-1} was attributed to H–O–H bending vibration, which was assigned to a small amount of H_2O in the ZnO nanocrystals [39].

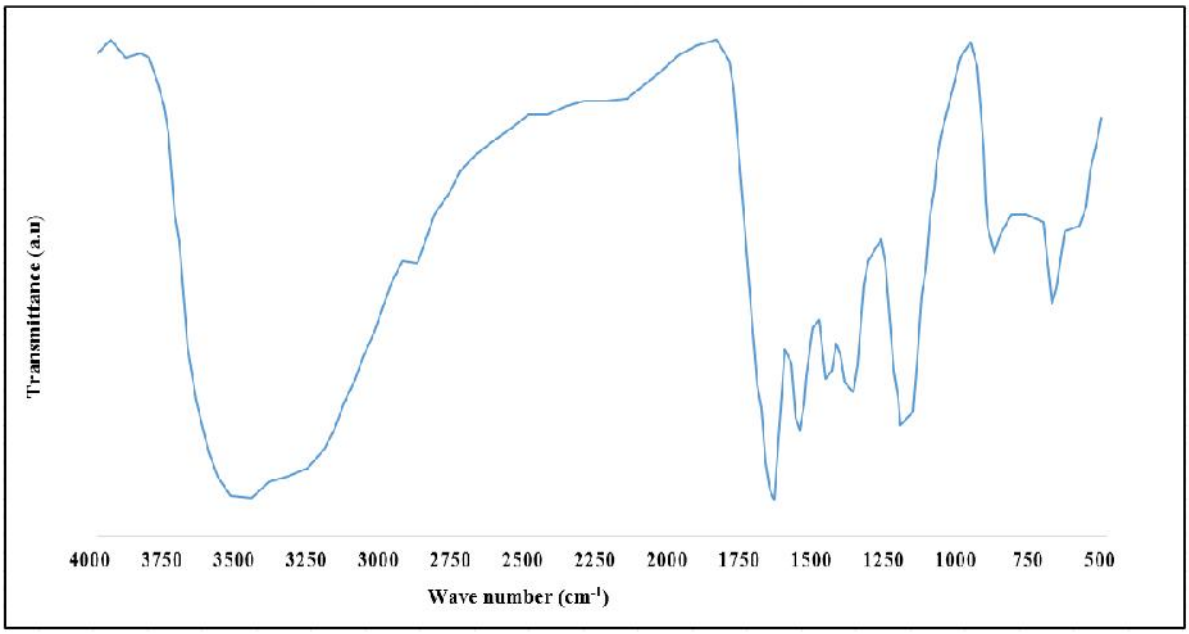

Fig. 8. FT-IR spectra of CuO/ZnO photocatalyst

The weak bands at 832cm^{-1} and 623 cm^{-1} were assigned to the vibrational frequencies due to the change in the microstructural features by the addition of Cu into the Zn–O lattice. The Zn–O bond was assigned to the stretching frequency at 550 cm^{-1} for pure ZnO which was shifted to a higher frequency as 550 cm^{-1}. The copper atom was slightly lighter than the Zn atom; so according to the well-established theories of vibrational modes in mixed crystals, the substitution should result in an upward shift of the fundamental transverse optical phonon mode [40]. The observed upward shift in the present system was consistent with the results given by Singhal et al. [41]. The frequency shift towards the lower side revealed the substitution of a Cu^{2+} ion into the Zn–O lattice. Also, the additional weak band was seen at 2851 cm^{-1}.

3.3. Evaluation of photocatalytic efficiency of CuO/ZnO

Table 3 shows the design of experiments and the corresponding responses which were determined using a UV–vis spectrophotometer. After each experiment, samples were centrifuged for 20 minutes and then, the transparent part of solution was analyzed by a UV-Vis spectrophotometer (UV-Vis. Shimadzu 1650- PC Spectrophotometer). Firstly, the calibration curve of 4-CP in the studied range was prepared. The maximum absorption peaks of 4-CP were disclosed at λ_{max}=225 and 280 nm. These peaks were used in the measurement of 4-CP concentration in each test based on Equation (4), where C_0 and C_1 are initial and final 4-CP concentration, respectively.

$$\%\text{Degradation}=\frac{C_1-C_0}{C_0} \quad (4)$$

3.2.1. Statistical analysis

Figure 9 shows the t-values of the different factors effect and their interaction in the degradation of 4-CP. As can be seen, the time of irradiation played the most important role in the photocatalytic activity;also, the interaction between catalyst concentration and pH was low and the influences of other parameters on each other w were negligible. In addition, Table 4 shows the numerical value of these factors and indicates those used in the process model and considered as a percentage of error. The analysis of variance (ANOVA) was used to adjust the process model. ANOVA is a standard statistical technique used to interpret the experimental results, but you must make sure that the assumption of this method is established. To see how well the model satisfied the assumptions of the ANOVA, the plots of Normality and residual versus predicted values were analyzed. The normal probability plot, (Figure 10), indicated that the residuals follow a normal distribution; in which case, the points followed a straight line. This indicated that the model satisfied the assumption of ANOVA. The plot of the residuals versus the predicted response values (Figure 11) tested the assumption of constant variance.

Table 3. Design of experiments

Run	Factors				Response
	A	B	C	D	
	pollutant concentration (g/0.5L)	catalyst concentration (g/0.5L)	Time (min)	pH	Degradation Percent (%)
1	0.05	0.07	60.00	8.00	51
2	0.05	0.01	60.00	8.00	65
3	0.05	0.07	60.00	6.00	62
4	0.05	0.01	60.00	6.00	27
5	0.01	0.01	60.00	8.00	51
6	0.01	0.01	60.00	6.00	40
7	0.05	0.07	240.00	6.00	42
8	0.05	0.01	240.00	6.00	63
9	0.01	0.01	240.00	8.00	79
10	0.05	0.07	240.00	6.00	69
11	0.05	0.07	240.00	8.00	80
12	0.01	0.01	60.00	8.00	55
13	0.01	0.07	240.00	6.00	85
14	0.05	0.07	60.00	6.00	45
15	0.01	0.07	60.00	8.00	71
16	0.01	0.07	240.00	8.00	95

The plot showed the constant range of residuals across the graph which was welcomed and warranted no need for a transformation to minimize personal error. The ANOVA proposed model was as shown in Equation 5:

$$Y=-8.70-400.00A+516.66B+0.13C+7.00D-33.33BD \quad (5)$$

Where Y represents degradation percent (%) and A, B, C, D, BD is pollutant concentration, catalyst concentration, time, pH and interaction between catalyst concentration and pH, respectively. Table 5 shows the results of ANOVA and indicates that this model was significant. Equation 4 was used to predict the photodegradation efficiencies of 4-CP by the CuO-ZnO. By using the resulted equation (Equation 4), the predicted values versus the corresponding experimental results of the photodegradation of 4-CP is plotted in Figure 12. The results confirm that the predicted photocatalytic degradation efficiencies from the model are in good agreement with the experimental results. The correlation coefficient (R^2) value is usually in the range 0-1. The model is stronger and can better predict the responses when R^2 values are closer to 1. The results of this study indicated that the values of R^2 were found to be 0.99.

Table 4. Parameters of model and error

	Term	Effect	Sum of Squares	% Contribution
Model	A-Pollutant	-16	1024	20.27
Model	B-Catalyst concentration	17	1156	22.89
Model	C-Time	24.25	2352.25	46.57
Model	D-PH	11	484	9.58
Error	AB	-1	4.00791922	0.079
Error	AC	0.75	2.25	0.045
Error	AD	-0.5	1.00197981	0.020
Error	BC	0.75	2.25	0.045
Model	BD	-2	16.00	0.32
Error	CD	0.75	0316769	0.045
Error	ABC	0.75	2.25	0.04
Error	ABD	0	2.25	0
Error	ACD	0.25	0	0.0049
Error	BCD	0.75	0.25	0.045
Error	ABCD	0.75	2.25	0.045

Table 5. Analysis of variance

Source	Sum of Squares	DF	Mean Square	F Value	p-value Prob > F	
Model	5032.25	5	1006.45	536.77	<0.0001	Significant
A-Pollutant Concentration	1024.00	1	1024.00	546.13	<0.0001	
B-Catalyst Concentration	1156.00	1	1156.00	616.53	<0.0001	
C-Time	2352.25	1	2352.25	1254.53	<0.0001	
D-PH	484.00	1	484.00	258.13	<0.0001	
BD	16.00	1	16.00	8.53	0.0153	
Residual	18.75	10	1.88			
Cor Total	5051.00	15				

R^2=0.9963, adjusted R^2=0.9944

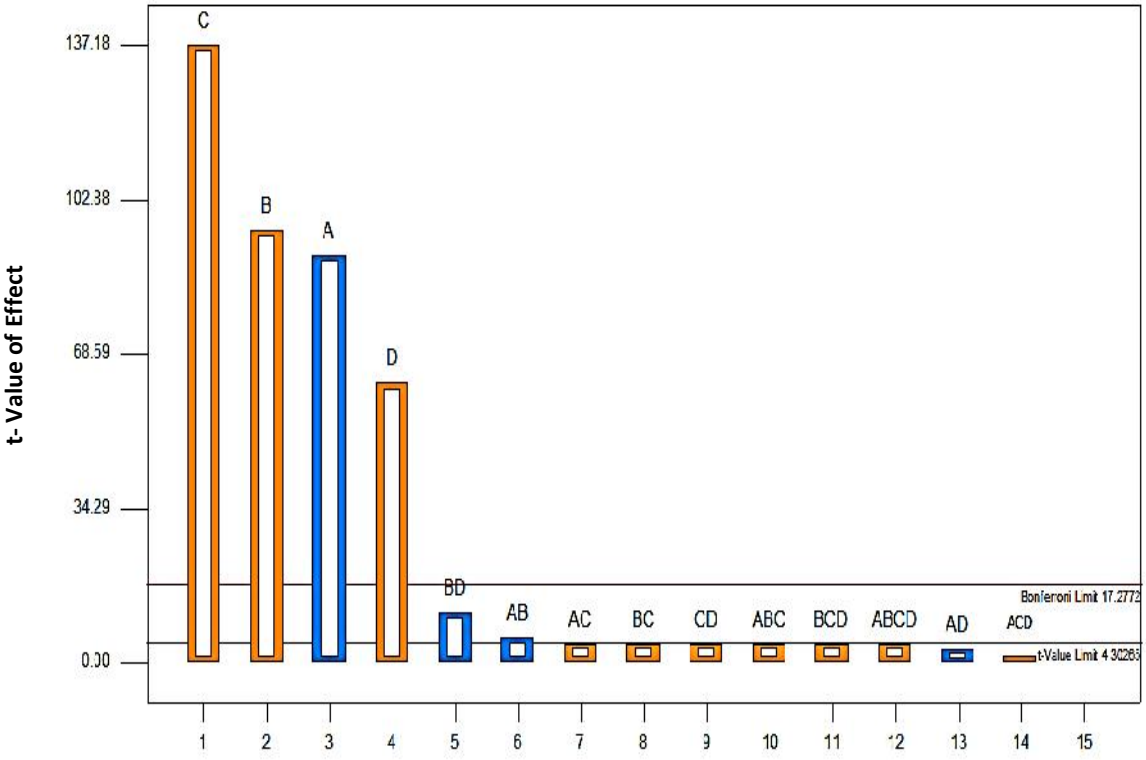

Fig. 9. T-value of different factors effect

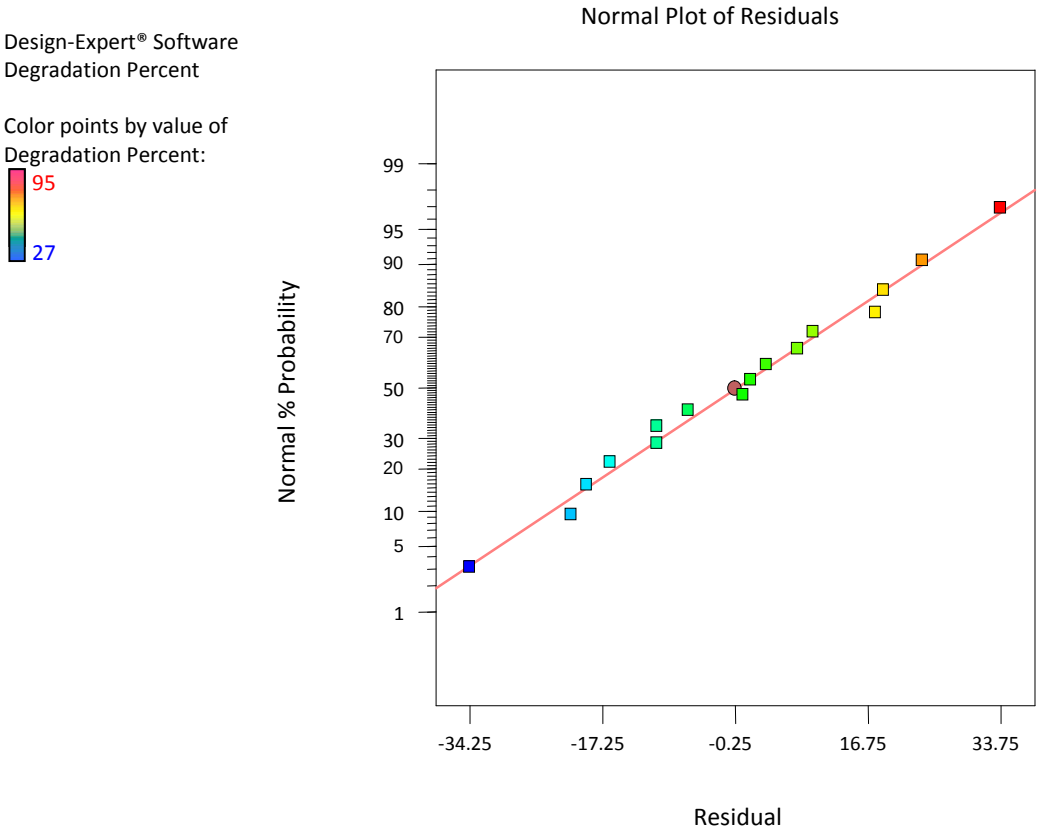

Fig. 10. Normal plot of residuals

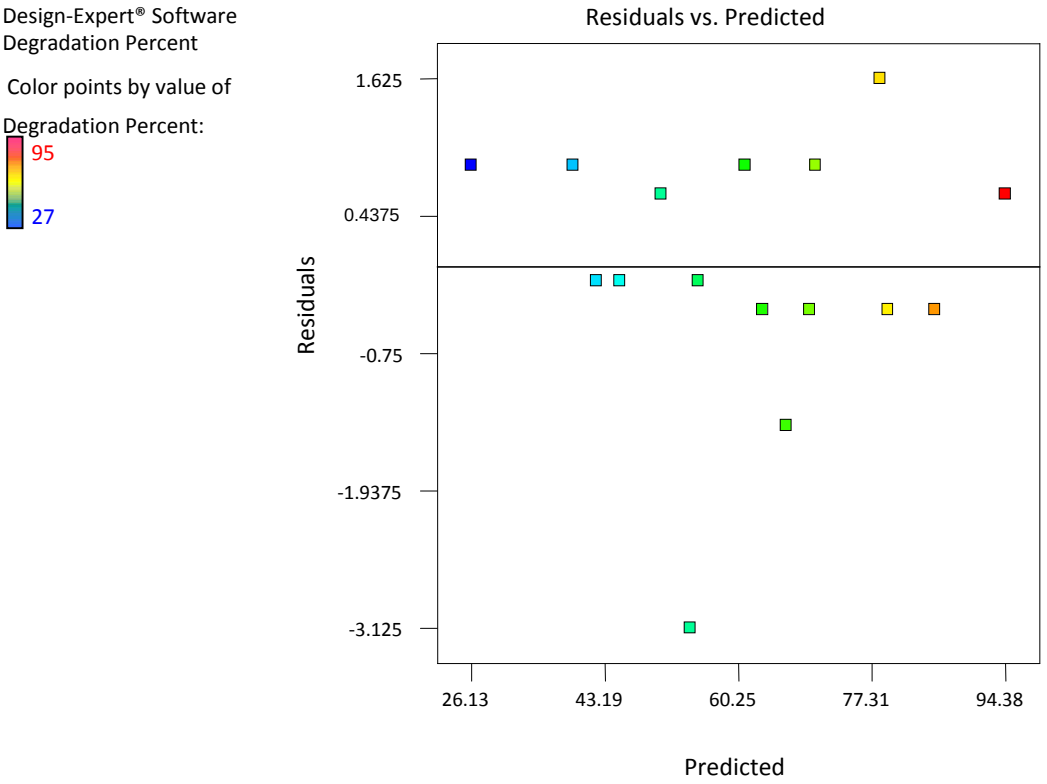

Fig. 11. Plot of residuals versus model predicted values

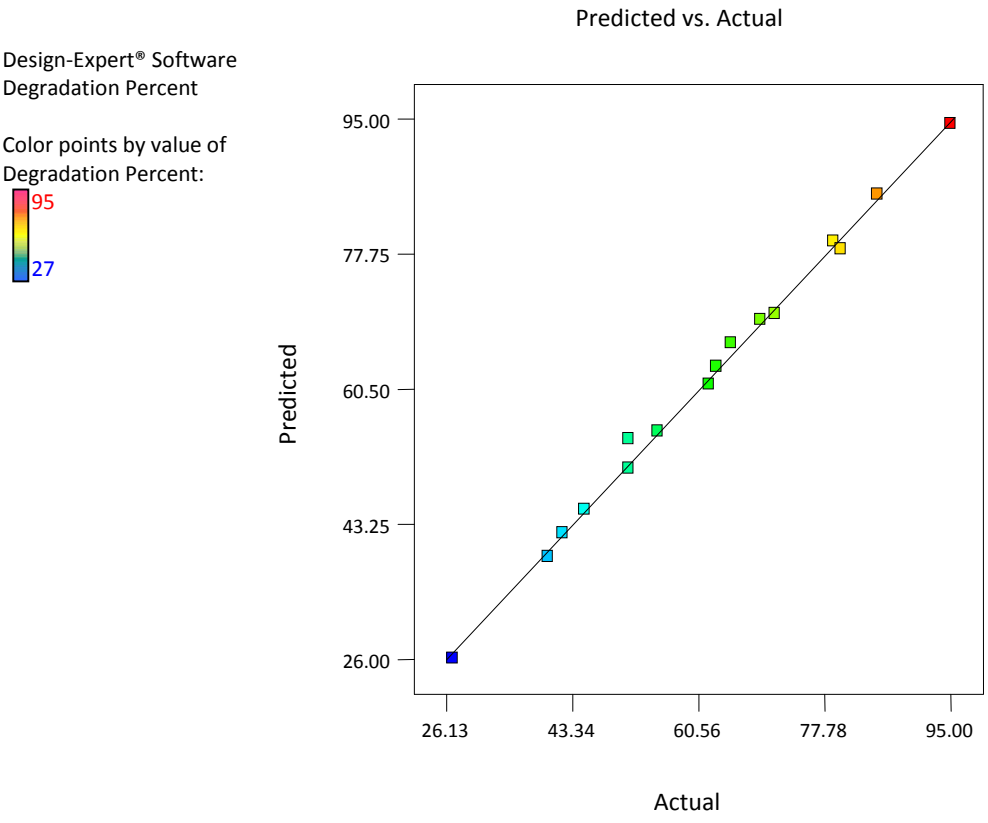

Fig. 12. Comparison between predicted values and experimental values calculated by software (predicted R^2=0.9905)

3.2.2. Effect of the initial concentration of 4-CP on photocatalytic activity

Under the same conditions (catalyst concentration: 0.07 g/L, time of irradiation: 240 min, pH=8), the photocatalytic degradation efficiency of 4-CP was decreased from 95% to 80% with the increase of the initial 4-CP concentration from 0.01 to 0.05 g/L. This may be due to the fact that as the initial concentration of 4-CP increased, more molecules of the pollutant occupied a greater area of the catalyst surface; but the number of $OH^{\cdot}$ and $\dot{O}_2^{-}$ radicals formed on the catalyst surface and the irradiation time were constant. The activation of TiO_2 by UV light can be represented by the following steps [42]:

$$ZnO + h\vartheta \rightarrow e_{CB^-} + h_{VB}^{+} \quad (6)$$

$$H_2O + h_{VB}^{+} \rightarrow \dot{OH} + H^{+} \quad (7)$$

$$O_2\ ads\ + eCB^{-} \rightarrow \dot{O}_2^{-} \quad (8)$$

$$OH_{(ads)}^{-} + h_{VB}^{+} \rightarrow \dot{O}H_{(ads)} \quad (9)$$

Therefore, by reducing the relative number of oxidizing radicals for trapping 4-CP molecules, the photocatalytic efficiency decreases. Also, with increasing concentrations of 4-CP, the photons get interrupted before they can reach the photocatalyst surface; thus, the absorption of photons by the photocatalyst decreases and photocatalytic efficiency was reduced [43-45]. Hence, at the given conditions, the optimum concentration of 4-CP was selected as 0.02 g/L.

3.2.3. Effect of pH on the photocatalytic activity

The pH dependence of the activity of heterogeneous photocatalysts is undeniable. The adsorption of organic pollutants on the catalyst surface is affected by its surface charge, which is related to the pH. The variation in pH entails an alteration in the properties of the catalyst–liquid interface, primarily associated with the acid–base equilibrium of the adsorbed hydroxyl groups. Under light irradiation, the electrons in the valence band will be excited to the conduction band to form holes. The surface of the photocatalyst will be negatively charged under the weak basic environment, which is favorable to the transfer of holes to the surface, where the hole can react with electron donors such as OH^{-} or H_2O to generate highly oxidizing $OH^{\cdot}$ radicals. Therefore, the formation of a hydroxyl radical from OH^{-} is enhanced at a higher pH, a chemically stable pH range for ZnO is 4 ≤ pH ≤ 14 [45]. The results of researches showed that ZnO is not capable of the degradation of 4-CP at a pH of 4. According to Equation 10, this may be due to the loss of ZnO at a low pH in an aqueous acidic media [8,10].

$$ZnO + 2H^{+} \rightarrow Zn^{2+} + H_2O \quad (10)$$

According to Equation 11, in an aqueous solution, ZnO is mainly in a hydrolysed form:

$$ZnO + H_2O \rightarrow Zn - OH + OH^{-} \quad (11)$$

Moreover, due to the alkaline dissolution of ZnO at pH>10, the stability of ZnO may not beguaranteed.

$$ZnO + H_2O + 2OH^{-} \rightarrow [Zn\ \ OH\ _2]^{2+} \quad (12)$$

The point of zero charge (isoelectric point) for ZnO is at pH_{pzc}=9. Below pH_{pzc}, a hydrolysed form of ZnO (Zn-OH) can be protonated to $ZnOH_2^{+}$ or deprotonated to $Zn–O^{-}$ above pHpzc [46]. Below a pH of 9, active sites on the catalyst surface are positively charged and largely covered by 4-CP anions; thus, the surface concentration of OH^{-} and $OH^{\cdot}$ are low and consequently, photocatalytic efficiency decreases at an acidic pH. On the other hand, above pH 9, the hydroxyl radical concentration is high while the concentration of the 4-CP is low on the surface. In addition, 4-CP is deprotonated above pH 9, and prevents the adsorption of 4-CP. Consequently, the surface concentration of the 4-CP decreases, which results in the decrease of photocatalytic degradation. Electrostatic repulsion between deprotonated 4-CP and negatively charged catalyst surface (covered by metal-bond OH^{-}) prevents adsorption of 4-CP. So the optimum pH is the moderate surface concentration of 4-CP and OH^{-}. Also, it should be noted that the dissociation of 4-CP in the basic medium is better done and 4-CP in an anionic form can easily get to the catalyst surface. Equation 13 shows 4-CP ionic dissociation equilibrium [47].

$$C_6H_4ClOH \leftrightarrow C_6H_4ClO^{-} + H^{+} \quad (13)$$

Similar results have also been reported by other researchers [48-50].

3.2.4. Effect of catalyst concentration on degradation of 4-CP and its interaction with pH

From Figure 9, it can be understood that the catalyst concentration and pH have little interaction, while influences of other parameters on each other are negligible. Both the 3-D and contour plots show the simultaneous effect of the catalyst concentration and pH on the photodegradation efficiency of 4-CP, while two other variables (initial concentration of pollutant and time of irradiation) are kept at their optimum values. As can be seen in Figure 13, with increasing of catalyst concentration from 0.01 to 0.07, the percent of the degradation increase from 79% to 95%. When the concentration of catalyst increases, the generation of hydroxyl radicals were increased and it converts organic pollutant to mineral products such as CO_2 and H_2O. On the other hand, generated hydroxyl radicals increase pH and cause an interaction between pH and catalyst concentration. It should be noted that when the catalyst concentration is increased so that the solution is not homogeneous and becomes turbid, the penetration of light intercept and degradation efficiency decrease [51-54].

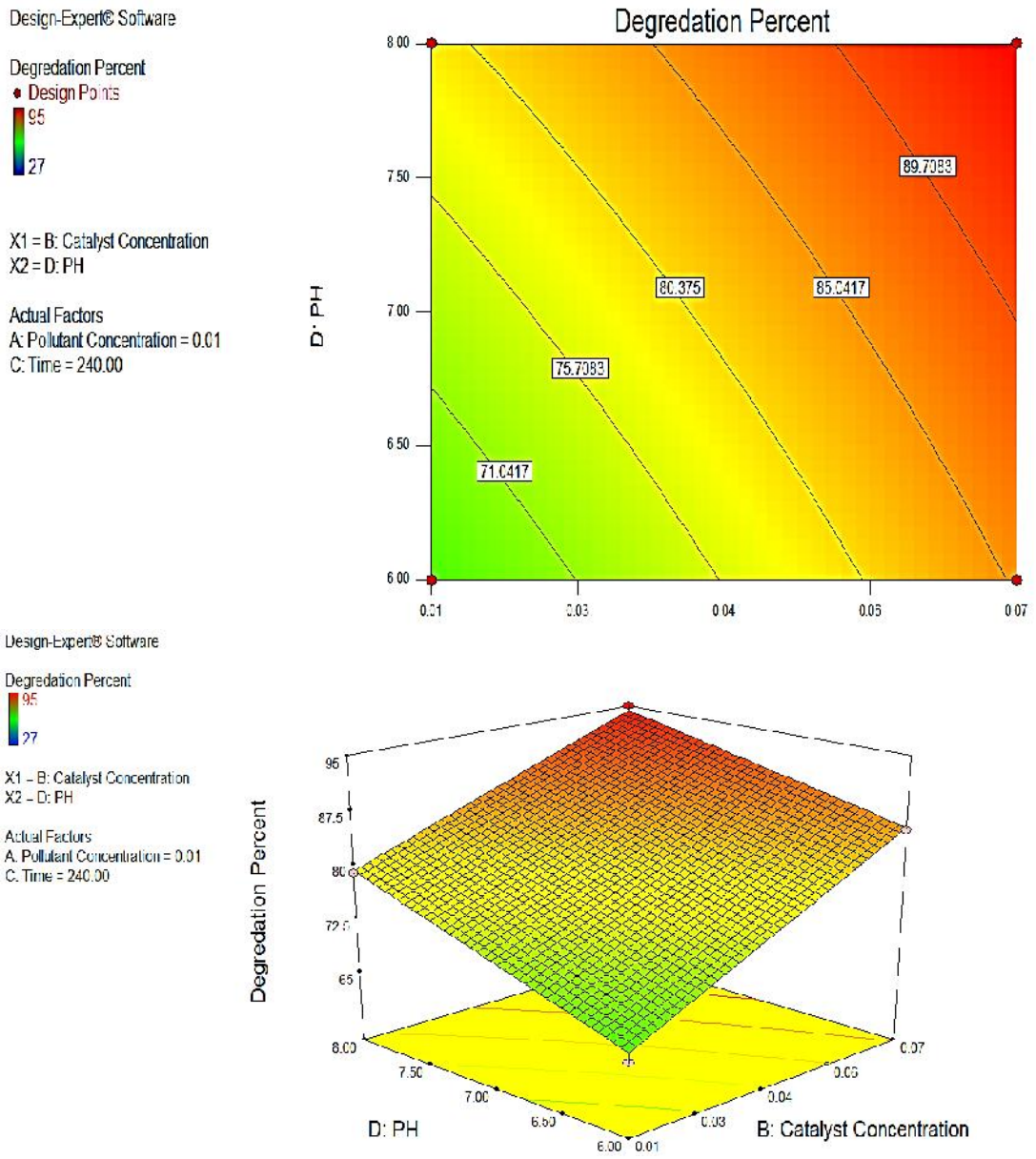

Fig. 13. The response surface and contour plots of the degradation efficiency of 4-CP by CuO-ZnO coupled as a function of catalyst concentration and pH

3.2.5. The effect of irradiation time on photocatalytic a6ctivity

The effect of irradiation time on the photocatalytic degradation of 4-CP was investigated from 60 to 240 min at a 4-CP concentration of 0.01 g/L, catalyst dosage of 0.07 g/L, and pH value of 8.0. As can be seen in Figure 9, the time of irradiation was the most important factor on the photodegradation of 4-CP. Increasing of degradation efficiency from 71 to 95% with an increase in the time of irradiation from 60 to 240 min under the given condition suggests that the CuO-ZnO catalyst has remarkable and persistent photocatalytic activity.

4. Conclusions

The overall results were classified as follows:
Synthesis of nanostructures ZnO:

- XRD pattern showed that synthesized ZnO was in good agreement with the reference pattern for the wertzite hexagonal structure. In addition, the peaks in this pattern showed no impurities.
- Using the Debye-Sherrer Equation, the average crystallite size of synthesized ZnO particles was calculated at about 41 nm.
- SEM image demonstrated cauliflower-like and rod morphology.
- The dimensions of nano cauliflower-likes and

nanorods were estimated at about 85, 79 and 117 nm from the TEM image.

Doping ZnO with CuO:

- XRD pattern showed successful doping of a CuO cluster with a monoclinic structure on the ZnO nanostructures.
- The average crystallite size of CuO/ZnO was calculated at about 36nm from the Debye-Sherrer formula that was smaller than pure ZnO. Thus, CuO/ZnO provided a higher ratio of surface to volume and better adsorption of pollutant that resulted in an increase of photocatalytic efficiency.
- Using the results of UV-Vis DRS, the band gap of CuO/ZnO was calculated at about 2.9 eV from Touc's plot. A decrease of the band gap caused to increase of photocatalytic activity in the visible range.

Photocatalytic activity of CuO/ZnO:

- The effect of various parameters, including pollutant concentration, catalyst concentration, pH, and time of irradiation on degradation efficiency of 4CP was investigated and found that the time of irradiation was the most important factor with 46.57% effect; the catalyst concentration and pH had a very low interaction and the influences of parameters on each other were negligible.
- The calculated result from the model was in good agreement with experimental results (R^2=0.99).
- An increase in catalyst concentration up to homogenous solution resulted in an increase in the number of active sites in the surface of the catalyst.
- In a specified concentration of catalyst and irradiation time, an increase in initial 4-CP concentration decreased the photodegradation of 4-CP.
- The photodegradation of 4-CP by CuO/ZnO in the basic mediums was higher than the acidic medium.
- An increase in the time of irradiation under the given condition suggests that the CuO-ZnO catalyst has remarkable and persistent photocatalytic activity.
- The optimal experimental conditions for 4-CP concentration (0.01 g/L) were found at an initial pH=8 and catalyst loading of 0.07 g/L. The results showed that Cu-ZnO can remove 95% of 4-chlorophenol from water under optimal conditions after 4 hr of irradiation.

References

[1] Wang, Q., Geng, B., Wang, S. (2009). ZnO/Au hybrid nanoarchitectures: wet-chemical synthesis and structurally enhanced photocatalytic performance. *Environmental science and technology*, *43*(23), 8968-8973.

[2] Jain, A. K., Gupta, V. K., Jain, S., Suhas. (2004). Removal of chlorophenols using industrial wastes. *Environmental science and technology*, *38*(4), 1195-1200.

[3] Chen, D., Ray, A. K. (1999). Photocatalytic kinetics of phenol and its derivatives over UV irradiated TiO_2. *Applied Catalysis B: Environmental*, *23*(2), 143-157.

[4] Sherrard, K. B., Marriott, P. J., Amiet, R. G., McCormick, M. J., Colton, R., Millington, K. (1996). Spectroscopic analysis of heterogeneous photocatalysis products of nonylphenol-and primary alcohol ethoxylate nonionic surfactants. *Chemosphere*, *33*(10), 1921-1940.

[5] Selcuk, H., Bekbolet, M. (2008). Photocatalytic and photoelectrocatalytic humic acid removal and selectivity of TiO 2 coated photoanode. *Chemosphere*, *73*(5), 854-858.

[6] Devi, L. G., Murthy, B. N., Kumar, S. G. (2009). Heterogeneous photo catalytic degradation of anionic and cationic dyes over TiO_2 and TiO_2 doped with Mo 6+ ions under solar light: correlation of dye structure and its adsorptive tendency on the degradation rate. *Chemosphere*, *76*(8), 1163-1166.

[7] Yamazaki, S., Fujiwara, Y., Yabuno, S., Adachi, K., Honda, K. (2012). Synthesis of porous platinum-ion-doped titanium dioxide and the photocatalytic degradation of 4-chlorophenol under visible light irradiation.*Applied catalysis B: Environmental*, *121*, 148-153.

[8] Gaya, U. I., Abdullah, A. H., Zainal, Z., Hussein, M. Z. (2009). Photocatalytic treatment of 4-chlorophenol in aqueous ZnO suspensions: Intermediates, influence of dosage and inorganic anions. *Journal of hazardous materials*, *168*(1), 57-63.

[9] Ou, H. H., Lo, S. L., Wu, C. H. (2006). Exploring the interparticle electron transfer process in the photocatalytic oxidation of 4-chlorophenol. *Journal of hazardous materials*, *137*(3), 1362-1370.

[10] Behnajady, M. A., Modirshahla, N., Hamzavi, R. (2006). Kinetic study on photocatalytic degradation

of CI Acid Yellow 23 by ZnO photocatalyst. *Journal of hazardous materials*, *133*(1), 226-232.

[11] Salehi, K., Daraei, H., Teymouri, P., Maleki, A. (2014). Hydrothermal synthesis of surface-modified copper oxide-doped zinc oxide nanoparticles for degradation of acid black 1: Modeling and optimization by response surface methodology. *Journal of advances in environmental health research*, *2*(2), 101-109.

[12] Zhou, G., Deng, J. (2007). Preparation and photocatalytic performance of Ag/ZnO nano-composites. *Materials science in semiconductor processing*, *10* (2), 90-96.

[13] Irimpan, L., Krishnan, B., Nampoori, V. P. N., Radhakrishnan, P. (2008). Luminescence tuning and enhanced nonlinear optical properties of nanocomposites of ZnO–TiO_2. *Journal of colloid and interface science*, *324*(1), 99-104.

[14] Georgieva, J., Armyanov, S., Valova, E., Poulios, I., Sotiropoulos, S. (2007). Enhanced photocatalytic activity of electrosynthesised tungsten trioxide–titanium dioxide bi-layer coatings under ultraviolet and visible light illumination. *Electrochemistry communications*, *9*(3), 365-370.

[15] Wang, C., Wang, X., Xu, B. Q., Zhao, J., Mai, B., Peng, P. A., Fu, J. (2004). Enhanced photocatalytic performance of nanosized coupled ZnO/SnO_2 photocatalysts for methyl orange degradation. *Journal of Photochemistry and photobiology A: Chemistry*, *168*(1), 47-52.

[16] Sakthivel, S., Geissen, S. U., Bahnemann, D. W., Murugesan, V., Vogelpohl, A. (2002). Enhancement of photocatalytic activity by semiconductor heterojunctions: α-Fe_2O_3, WO_3 and CdS deposited on ZnO. *Journal of photochemistry and photobiology A: chemistry*, *148*(1), 283-293.

[17] Yoon, D. H., Yu, J. H., Choi, G. M. (1998). CO gas sensing properties of ZnO–CuO composite. *Sensors and actuators B: Chemical*, *46*(1), 15-23.

[18] Reitz, T. L., Ahmed, S., Krumpelt, M., Kumar, R., Kung, H. H. (2000). Characterization of CuO/ZnO under oxidizing conditions for the oxidative methanol reforming reaction. *Journal of molecular catalysis A: chemical*, *162*(1), 275-285.

[19] Choi, J. D., Choi, G. M. (2000). Electrical and CO gas sensing properties of layered ZnO–CuO sensor. *Sensors and actuators B: Chemical*, *69*(1), 120-126.

[20] Udom, I., Ram, M. K., Stefanakos, E. K., Hepp, A. F., Goswami, D. Y. (2013). One dimensional-ZnO nanostructures: synthesis, properties and environmental applications. *Materials science in semiconductor processing*, *16*(6), 2070-2083.

[21] Udom, I., Ram, M. K., Stefanakos, E. K., Hepp, A. F., Goswami, D. Y. (2013). One dimensional-ZnO nanostructures: synthesis, properties and environmental applications. *Materials science in semiconductor processing*,*16*(6), 2070-2083.

[22] Tao, Y. M., Ma, S. Y., Chen, H. X., Meng, J. X., Hou, L. L., Jia, Y. F., Shang, X. R. (2011). Effect of the oxygen partial pressure on the microstructure and optical properties of ZnO: Cu films. *Vacuum*, *85*(7), 744-748.

[23] Wang, X. B., Song, C., Geng, K. W., Zeng, F., Pan, F. (2007). Photoluminescence and Raman scattering of Cu-doped ZnO films prepared by magnetron sputtering. *Applied surface science*, *253*(16), 6905-6909.

[24] Chang, Y. S., Chien, C. T., Chen, C. W., Chu, T. Y., Chiang, H. H., Ku, C. H., Chen, K. H. (2007). Structural and optical properties of single crystal $Zn_{1-x}Mg_xO$ nanorods—experimental and theoretical studies. *Journal of applied physics*, *101*(3), 033502–033509.

[25] Reddy, A. J., Kokila, M. K., Nagabhushana, H., Chakradhar, R. P. S., Shivakumara, C., Rao, J. L., Nagabhushana, B. M. (2011). Structural, optical and EPR studies on ZnO: Cu nanopowders prepared via low temperature solution combustion synthesis. *Journal of alloys and compounds*, *509*(17), 5349-5355.

[26] Sonawane, Y. S., Kanade, K. G., Kale, B. B., Aiyer, R. C. (2008). Electrical and gas sensing properties of self-aligned copper-doped zinc oxide nanoparticles. *Materials research bulletin*, *43*(10), 2719-2726.

[27] Thennarasu, G., Sivasamy, A., Kavithaa, S. (2013). Synthesis, characterization and catalytic activity of nano size semiconductor metal oxide in a visible light batch slurry photoreactor. *Journal of molecular liquids*, *179*, 18-26.

[28] Jonidi-Jafari, A., Shirzad-Siboni, M., Yang, J. K., Naimi-Joubani, M., Farrokhi, M. (2015). Photocatalytic degradation of diazinon with illuminated ZnO–TiO_2 composite. *Journal of the Taiwan institute of chemical engineers*, *50*, 100-107.

[29] Naimi-Joubani, M., Shirzad-Siboni, M., Yang, J. K., Gholami, M., Farzadkia, M. (2015). Photocatalytic reduction of hexavalent chromium with illuminated ZnO/TiO_2 composite. *Journal of industrial and engineering chemistry*, *22*, 317-323.

[30] Samarghandi, M. R., Yang, J. K., Lee, S. M., Giahi, O., Shirzad-Siboni, M. (2014). Effect of different type of organic compounds on the photocatalytic reduction of Cr (VI) in presence of ZnO nanoparticles. *Desalination and water treatment*, *52*(7-9), 1531-1538.

[31] Shirzad-Siboni, M., Farrokhi, M., Darvishi Cheshmeh Soltani, R., Khataee, A., Tajassosi, S. (2014). Photocatalytic reduction of hexavalent chromium over ZnO nanorods immobilized on kaolin. *Industrial and engineering chemistry research*, *53*(3), 1079-1087.

[32] Ahmed, S., Rasul, M. G., Brown, R., Hashib, M. A. (2011). Influence of parameters on the heterogeneous photocatalytic degradation of pesticides and phenolic contaminants in wastewater: a short review. *Journal of environmental management*, *92*(3), 311-330.

[33] Elghniji, K., Hentati, O., Mlaik, N., Mahfoudh, A., Ksibi, M. (2012). Photocatalytic degradation of 4-chlorophenol under P-modified TiO 2/UV system: Kinetics, intermediates, phytotoxicity and acute toxicity. *Journal of environmental sciences*, *24*(3), 479-487.

[34] Li, X., Hou, Y., Zhao, Q., Teng, W., Hu, X., Chen, G. (2011). Capability of novel ZnFe 2 O 4 nanotube arrays for visible-light induced degradation of 4-chlorophenol. *Chemosphere*, *82*(4), 581-586.

[35] Zak, A. K., Wang, H. Z., Yousefi, R., Golsheikh, A. M., Ren, Z. F. (2013). Sonochemical synthesis of hierarchical ZnO nanostructures. *Ultrasonics sonochemistry*, *20*(1), 395-400.

[36] Tauc, J., Menth, A. (1972). States in the gap. *Journal of non-crystalline solids*, *8*, 569-585.

[37] Abdollahi, Y., Abdullah, A. H., Zainal, Z., Yusof, N. A. (2011). Synthesis and characterization of Manganese doped ZnO nanoparticles. *International journal of basic and applied sciences*, *11*(4), 62-69.

[38] Nakamoto, K. (1986). Infrared and Raman spectra of inorganic and coordination compounds. John Wiley and Sons, Ltd.

[39] Reddy, A. J., Kokila, M. K., Nagabhushana, H., Chakradhar, R. P. S., Shivakumara, C., Rao, J. L., Nagabhushana, B. M. (2011). Structural, optical and EPR studies on ZnO: Cu nanopowders prepared via low temperature solution combustion synthesis. *Journal of alloys and compounds*, *509*(17), 5349-5355.

[40] Taylor, D. W., Elliott, R. J. (1988). Optical properties of mixed crystals, North-Holland.

[41] Singhal, S., Kaur, J., Namgyal, T., Sharma, R. (2012). Cu-doped ZnO nanoparticles: synthesis, structural and electrical properties. *Physica B: Condensed matter*, *407*(8), 1223-1226.

[42] Selvam, N. C. S., Narayanan, S., Kennedy, L. J., Vijaya, J. J. (2013). Pure and Mg-doped self-assembled ZnO nano-particles for the enhanced photocatalytic degradation of 4-chlorophenol. *Journal of environmental sciences*, *25*(10), 2157-2167.

[43] Pardeshi, S. K., Patil, A. B. (2009). Solar photocatalytic degradation of resorcinol a model endocrine disrupter in water using zinc oxide. *Journal of hazardous materials*, *163*(1), 403-409.

[44] Behnajady, M. A., Modirshahla, N., Shokri, M. (2004). Photodestruction of Acid Orange 7 (AO7) in aqueous solutions by UV/H_2O_2: influence of operational parameters. *Chemosphere*, *55*(1), 129-134.

[45] Rabindranathan, S., Devipriya, S., Yesodharan, S. (2003). Photocatalytic degradation of phosphamidon on semiconductor oxides. *Journal of hazardous materials*, *102*(2), 217-229.

[46] Kosmulski, M. (2006). pH-dependent surface charging and points of zero charge: III. Update. *Journal of colloid and interface science*, *298*(2), 730-741.

[47] Liu, F., He, G., Zhao, M., Qu, M., Huang, L. (2011). Electrochemical behaviors of chlorophenol aqueous solutions at boron- doped diamond electrode. *Open materials science journal*, *5*, 35-39.

[48] Zhang, D. (2010). Synthesis and characterization of ZnO-doped cupric oxides and evaluation of their photocatalytic performance under visible light. *Transition metal chemistry*, *35*(6), 689-694.

[49] Doong, R. A., Chen, C. H., Maithreepala, R. A., sulfide on the photocatalytic degradation of 2-chlorophenol in titanium dioxide suspensions. *Water research*, *35*(12), 2873-2880.

[50] Baruah, S., Dutta, J. (2009). Hydrothermal growth of ZnO nanostructures. *Science and technology of advanced materials*, *10*(1), 1-18

[51] Daneshvar, N., Salari, D., Khataee, A. R. (2004). Photocatalytic degradation of azo dye acid red 14 in water on ZnO as an alternative catalyst to TiO_2. *Journal of photochemistry and photobiology A: chemistry*, *162*(2), 317-322.

[52] Rabindranathan, S., Devipriya, S., Yesodharan, S. (2003). Photocatalytic degradation of phosphamidon on semiconductor oxides. *Journal of hazardous materials*, *102*(2), 217-229.

[53] Shankar, M. V., Cheralathan, K. K., Arabindoo, B., Palanichamy, M., Murugesan, V. (2004). Enhanced photocatalytic activity for the destruction of monocrotophos pesticide by TiO_2/Hβ. *Journal of molecular catalysis A: Chemical*, *223*(1), 195-200.

[54] Körbahti, B. K., Rauf, M. A. (2008). Response surface methodology (RSM) analysis of photoinduced decoloration of toludine blue. *Chemical engineering journal*, *136*(1), 25-30.